Data-driven machine learning meta-analysis of process–property relationships in polymer additive manufacturing: A case study on FFF-printed PEEK

Huilong Fu[1], Navid Zobeiry[1*]

[1] University of Washington, Seattle, WA 98195, USA

navidz@uw.edu

Peer-reviewed Version of Record: Fu, H., and Zobeiry, N. (2026). Data-driven machine learning meta-analysis of process-property relationships in polymer additive manufacturing: A case study on FFF-printed PEEK. *Journal of Manufacturing Processes, 163, 100-113.*
https://doi.org/10.1016/j.jmapro.2026.02.044

ABSTRACT

Polymers are widely used in 3D printing technologies such as fused filament fabrication (FFF), where process parameters significantly influence the structure and performance of parts. Establishing process–property relationships is challenging due to the high dimensionality of the process space, limited and sparse data, and heterogeneity in the literature. We present a literature-driven meta-analysis focused on process–property measurements of FFF parts made from polyether ether ketone (PEEK). A dataset of 188 data points from 12 studies is compiled to examine the effects of nine printing parameters on ultimate tensile strength (UTS) of printed coupons. We train neural-network models and apply global sensitivity analysis (Sobol indices). To improve robustness and extract higher-order patterns, we adopt an ensemble strategy, training over 1,000 networks and selecting the top five based on performance metrics. This explainable AI (XAI) workflow quantifies both first-order and total-effect contributions; results show that while UTS is sensitive to parameters such as infill percentage and printing speed, sensitivity is significantly amplified when accounting for coupled interactions among parameters, elevating the influence of variables like nozzle temperature. The study provides a transferable, XAI framework that quantifies uncertainty and reveals higher-order interactions from literature-derived datasets, enabling data-driven process optimization in additive manufacturing.

Keywords: Fused Filament Fabrication (FFF); PEEK; Explainable AI (XAI); Global Sensitivity Analysis; Sobol Indices; Process–Property Relationships

VOR: doi.org/10.1016/j.jmapro.2026.02.044

1 INTRODUCTION

Three-dimensional (3D) printing, also known as additive manufacturing (AM), has revolutionized manufacturing, enabling complex parts to be fabricated with high precision and minimal material waste [1, 2]. First patented in 1986, stereolithography (SLA) allows objects to be printed layer-by-layer by applying ultraviolet light to photopolymer resins [3]. Since then, various 3D printing methods such as selective laser sintering (SLS) and selective laser melting (SLM) [4], electron beam melting (EBM) [5, 6], binder jetting (BJ) [7], fused filament fabrication (FFF) or fused deposition modeling (FDM®, trademarked by Stratasys) [8, 9] have been developed. The evolution of 3D printing technologies has expanded the range of printable materials, including polymers, concretes, metals, ceramics, and composites.

Despite these advances, one of the central challenges across 3D printing technologies is the difficulty of establishing reliable process–property relationships. In theory, the mechanical performance of printed parts—such as tensile strength or fatigue life—can be tailored through careful control of process conditions. In practice, however, this relationship is highly complex and often non-intuitive due to coupled interactions between multiple parameters, and the inherent variability of AM processes. Different additive manufacturing techniques involve distinct sets of processing parameters that significantly influence the microstructure, defect distribution, residual stresses, and ultimately the mechanical performance of the final parts. During SLM with metals, powders are melted by laser to build 3D objects layer-by-layer while the unmelted powders act as support material. The laser power intensity, scanning speed, layer height, powder size distribution, and other factors directly affect the structure and properties of the 3D-printed parts [5]. In FDM/FFF, thermoplastic polymer filament is melted and extruded through a hot nozzle to be deposited on a build plate. The nozzle temperature, printing speed, platform/bed temperature and cooling fan speed are among the significant factors that affect the porosity, surface roughness, crystal morphology, and mechanical properties of the coupons [10, 11].

A wide range of approaches have been used to study these process–property relationships. This includes traditional parametric studies such as one-factor-at-a-time (OFAT) and Design of Experiment (DOE). For example, varying the 3D-printing parameters one-at-a-time enabled Lee et al. [12] to study the effect of nozzle fan speed, sample location, and temperature history during FDM on the degree of crystallinity (DOC) and crystal morphology of PEEK. When three or more process parameters are involved, more complex DOE methods like orthogonal [13, 14], full factorial [15], central composite design (CCD) [16] or Taguchi L27 [11] are often used.

Along with these classical DOE approaches, there is a growing interest in applying machine learning (ML) to 3D-printing experimental data, and promising results have been reported. For example, printing with 316L stainless steel powder, Li et al. [17] developed an ensemble of three metamodels (namely, Gaussian Process Regression, Radial Basis Function, and Support Vector Regression) to predict and optimize multiple objectives including energy consumption, tensile strength and surface roughness, using SLM process parameters (i.e. layer thickness, laser power and scanning speed). In another study on FFF/FDM, Garg et al. [18] compared Genetic Programming [19] with artificial neural networks (NN), and second-order polynomial regression models to predict the compressive strength of the printed ABS parts using process parameters like air gap, raster angle and width. In the same study, analysis of variance (ANOVA) [20] was used to identify the most significant process parameters that affect the variance of the target response (compressive strength). Similar approach using NN and ANOVA could be found in [21]. In addition, Zhang et al. [22] combined in-process temperature and vibration sensing data with material properties and process parameters to train Long Short-Term Memory (LSTM) networks to predict the tensile strength of printed PLA parts.

However, despite these developments, it remains fundamentally challenging to apply such methods to small, sparse, and noisy datasets. Inherent variability arising from material properties, equipment and printer differences, process setups, operator control (human or robotic), environmental conditions, and the complexity of the underlying physics limits the reliability and generalizability of derived models. These challenges are further compounded when attempting to transfer insights across diverse datasets. Different printing methods involve distinct sets of printing parameters and material systems. For

 VOR: doi.org/10.1016/j.jmapro.2026.02.044

example, while lasers or electron beams can be used with metal powders, such high-intensity energy sources could degrade polymer filaments. Similarly, wire arc additive manufacturing [23] uses an entirely different heat source from FFF. Even within the same 3D printing category, differences in experimental design and setup often result in inconsistent outcomes (e.g. tensile strength, surface roughness, porosity, residual stress). Each study typically has its unique objectives, printing parameters, equipment, and research methodology, making many reported correlations context-specific, inconclusive, or not transferable. These issues pose a significant hurdle in leveraging the rapidly growing body of experimental data in the literature.

This limitation is particularly evident in the case of FFF with PEEK, a high-performance thermoplastic of growing interest. Several traditional analysis methods, along with ML methods have been proposed for this system. For example, Doyle et al. [24] designed a half-factorial DOE and applied multivariate linear regression to correlate tensile strength with nozzle temperature, bed temperature and printing speed. In addition, response surface methodologies (RSM), applying different DOE and polynomial fitting, are commonly used. For example, Wang et al. [25] used linear, quadratic or reduced cubic models to predict bending strength and modulus, compression strength and modulus, and then applied ANOVA to identify significant printing parameters. Similar approaches with RSM can be found in studies by Liu et al. [26] and Gao et al. [27]. In addition, Borah et al. [16] trained NN surrogate models to estimate the surface roughness and tensile strength of the 3D-printed PEEK coupons as a function of printing parameters.

Despite these successes, most existing models have been developed under isolated conditions with limited exploration of the process space. Consequently, their findings are often not generalizable to other experimental setups or higher-dimensional design spaces. To date, a robust and generalized machine learning framework for modeling process–property relationships in FFF—or other additive manufacturing methods—has yet to be established.

In this paper, we propose a framework for analyzing literature data using machine learning techniques, aiming to provide a more comprehensive understanding of process-property relationships in 3D printing with polymers. This approach is demonstrated through a focused literature survey on FFF with PEEK, where we compile and model experimental data from diverse sources. By identifying robust correlations and uncovering hidden patterns in this sparse and heterogeneous dataset, the proposed framework addresses key limitations of existing studies—namely, their reliance on isolated datasets and limited parameter spaces. Beyond prediction accuracy, trained NN models are used as surrogate models for explainable AI (XAI), applying Sobol global sensitivity analysis to quantify first-order and interaction effects among processing parameters, enabling transferable process insight rather than black-box fitting. Ultimately, this work contributes toward the development of more generalizable models to support improved process optimization, quality control, and manufacturing efficiency in polymer additive manufacturing.

2 LITERATURE SURVEY ON FFF WITH PEEK

For FFF with PEEK, numerous studies over the past decade have generated an extensive body of data encompassing various aspects of the process-structure-property relationship. In this section, we highlight selected experimental studies from which data points are extracted to compile a dataset for machine learning and global sensitivity analysis. The focus is on experimental studies reporting Ultimate Tensile Strength (UTS) alongside detailed 3D printing parameter values. Key FFF processing parameters are illustrated in Figure 1.

A typical commercial FFF printer (Intamsys Funmat HT) and associated slicer software (Intamsuite v4.3 [28]) are shown in Figure 2. This setup has been used in several studies included in the compiled dataset as well as others beyond [12]. The most commonly used tensile coupon geometries are ASTM D638-14 Type I and ISO527-2 Type I, though Type IV and V specimens from both standards also appear in the literature. Another equivalent standard, GB/T 1040, is also used in a few studies [10, 29]. A tensile testing coupon per ASTM D638-14 Type I is shown in Figure 3.

In this study, differences among FFF printers and coupon geometries are not explicitly considered in the analysis and are assumed to have secondary effect compared to the primary effects of printing parameters.

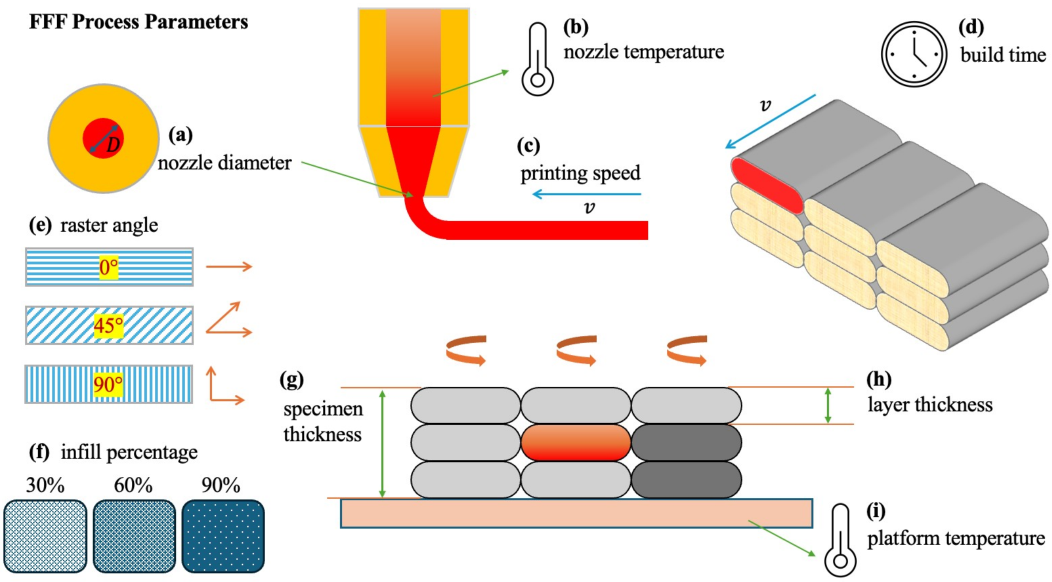

Figure 1 FFF process parameters for FFF with PEEK. The list is not exhaustive and only 9 parameters are illustrated based on the most available data in the compiled dataset: (a) nozzle diameter, (b) nozzle temperature, (c) printing speed, (d) build time, (e) raster angle, (f) infill percentage, (g) specimen thickness, (h) layer thickness, (i) platform temperature

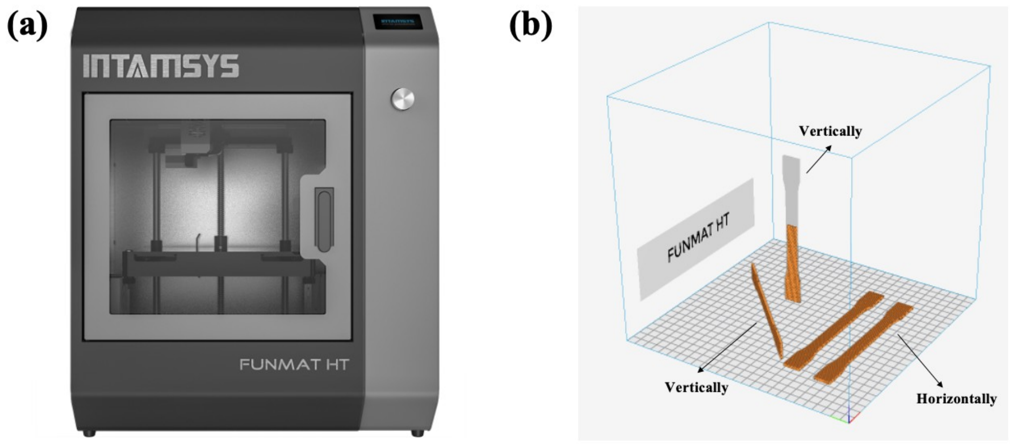

Figure 2 Example of Commercial FFF Hardware and Software: (a) Intamsys Funmat HT 3D-Printer, (b) Slicing Software Intamsuite V4.3 [28]

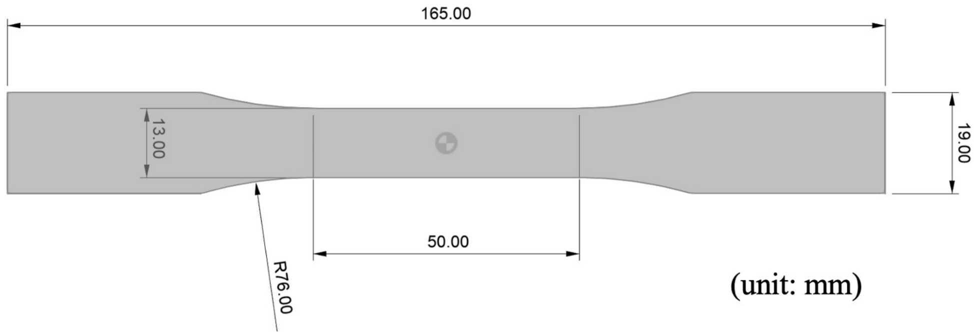

Figure 3 Tensile Testing Coupon per ASTM D638-14 Type I

PEEK, as a semicrystalline thermoplastic polymer, offers exceptional mechanical strength, thermal stability, and chemical resistance. Numerous studies have explored the process–structure–property relationships in PEEK parts fabricated by FFF. For example, Lee et al. [12] investigated the degree of crystallinity (DOC) and crystal morphology of FFF-printed PEEK under varying temperature histories and nozzle fan speeds. They observed that as fan speed increased, DOC dropped significantly —reaching as low as 11% at full fan speed—due to faster cooling rates during layer-by-layer deposition combined with short annealing time. This, in turn, can contribute to poor interlayer bonding and reduced mechanical properties. Another example is found in Qu et al. [30], who varied the ambient (chamber) temperature from 60 to 90 °C while keeping other printing parameters fixed. They reported noticeably enhanced interlayer bonding strength at higher temperatures, attributing this to reduced cross-sectional defects, increased melt flow capability, and improved interlaminar fusion. Lower temperature gradients and slower cooling rates were also cited as contributing factors. Although the cooling rate during the solidification of the molten polymer has been shown to significantly affect the DOC and final part properties —including interlayer strength —it is not directly controllable during 3D printing. Instead, it is indirectly governed by a combination of various process parameters such as nozzle temperature, bed temperature, chamber temperature, printing speed, layer-thickness, part geometry and others.

To compile a literature dataset for FFF-PEEK, twelve different studies were identified, each exploring different combinations of 3D-printing parameters, with all sources reporting UTS values. This enables a direct process-property comparison across these different data sources. A summary of selected findings from these studies is given below.

Zhao et al. [13] conducted orthogonal experiments and ANOVA while varying the nozzle temperature, ambient (chamber) and bed temperature for FFF-PEEK. They found that an optimal combination of these thermo-parameters could lead to improved interlayer bonding, lower porosity, and consequently, higher UTS. The ANOVA results indicated that the ambient temperature was relatively insignificant compared to the nozzle temperature and bed temperature.

Ding et al. [31] investigated the effects of build orientation (horizontal vs. vertical), and nozzle temperature on microstructure and mechanical properties of FFF-PEEK. As the nozzle temperature increased from 360 to 420 °C, the density of the printed coupon increased monotonically. However, tensile strength showed a non-monotonic trend with a dip around 380 °C before reaching a maximum at 420 °C. Larger voids and interlayer gaps were found in the SEM micrographs at lower nozzle temperatures, indicating reduced fusion and weaker interlayer bonding.

Sviridov et al. [32] used a set of FFF parameters to print PEEK coupons and compared the tensile properties with other studies. They found that the FFF-PEEK coupons had a UTS of 66.9 MPa, which was approximately 30% lower than cast (injection molding) samples. This is comparable to a ~30% reduction reported by Zhao et al. [13] and a ~20% reduction reported by Ding et al. [31], both comparing FFF-PEEK with injection molded PEEK.

Wang et al. [29] used finite element analysis (FEA) to simulate PEEK flow in the nozzle channel to optimize 3D printing parameters and improve the mechanical properties and surface quality of printed PEEK parts. The optimal designs were validated by physical experiments with varying nozzle temperature, printing speed, layer thickness and nozzle diameter. The cross-section (fractured surface) after tensile testing was smoother at the higher nozzle temperature (420-440 °C) with fewer voids between adjacent infill filaments in both horizontal and vertical directions, indicating a higher crystallinity and improved interlayer bonding compared to prints made at lower nozzle temperatures (380 °C). It was also reported that, when using nozzle diameters of 0.6 mm or 0.8 mm, a layer thickness equal to or greater than 0.35 mm would interrupt compaction and reduce interlayer bonding strength, leading to stratification and lower tensile strength. This effect was less pronounced with a 0.4 mm nozzle, where changes in layer thickness from 0.1 to 0.25 mm had minimal influence on tensile strength. Lastly, printing speed negatively affected the tensile strength with 0.6 and 0.8 mm nozzles, whereas the 0.4 mm nozzle showed improved tensile strength at moderate speeds (20-23 mm/s).

The same author group also investigated the 3D printing of two different PEEK composites reinforced with carbon fiber and glass fiber, respectively [33]. In both cases, increasing the fiber content from 5wt% to 15wt% led to higher porosity and reduced tensile strength. It was concluded that the added fibers increased the flow resistance of the molten polymer, restricted the polymer chain mobility, thereby resulted in poorer melt fluidity and a lower degree of crystallinity in the PEEK matrix.

Sikder et al. [34] conducted a comprehensive experimental study involving variations in nozzle, chamber and bed temperatures, layer height (thickness), printing speed and post-annealing conditions. A one-way analysis of variance (ANOVA) with Tukey's test was performed across all samples. SEM images revealed that air gaps, formed when adjacent filaments did not fully fuse, locally reduced the effective cross-sectional area and served as initiation sites for micro-cracks, ultimately leading to premature failure. At a chamber temperature of 25 °C, some coupons failed by interlayer delamination, whereas none of the coupons printed with 90 °C exhibited such failure. Another important observation was that both the color and degree of crystallinity of the printed PEEK coupons were affected by post-annealing. Coupons annealed at 200 °C for 2 hours, exhibited an 11% increase in average tensile strength and a 12.9% increase in compressive strength. In a related study, annealing with a temperature well above glass transition temperature of PEEK (~143 °C) and the cold crystallization temperature (~177 °C) for several hours increased the DOC from 13.3% to 37.4% [35].

Gao et al. [10] investigated the effects of nozzle temperature, printing speed, platform (bed) temperature, layer thickness and annealing temperature on the mechanical properties of FFF-PEEK coupons. Higher nozzle temperature improved the tensile strength and DOC, and reduced porosity percentage and average pore size. However, increasing platform temperature within the range of 125~140 °C did not result in noticeable changes in the aforementioned properties. Printing speed showed little impact on the tensile strength; however, the porosity percentage and pore size were positively correlated with the printing speed.

He et al. [14] found that lower printing speed and higher nozzle temperature were beneficial for the improvement of PEEK's mechanical properties. In both studies [10, 14], post-annealing helped improve both mechanical strength and DOC of the printed PEEK coupons.

Pulipaka et al. [11] used the Taguchi method for DOE along with ANOVA to measure which process parameters are more significant for the surface roughness and mechanical properties of FFF-PEEK. The ANOVA results showed that for bulk mechanical properties, the infill percentage, platform temperature, nozzle temperature and layer thickness were the most significant factors. The printing speed seemed to be insignificant within the tested range from 15-25 mm/s, which is similar to the observation by Gao et al. [10].

Vaglio et al. [15] found that highly porous structures were obtained at high printing speeds and large layer thicknesses, due to under-extrusion or insufficient flow capability of the melted PEEK. However, geometrical conformity and surface quality could be improved at lower nozzle temperatures, smaller layer thicknesses, and faster printing speeds.

Zhang et al. [36] extensively investigated the influence of raster (infill) angle, nozzle temperature, printing speed and layer thickness on the build time (BT), surface roughness (SR) and UTS of FFF-PEEK. They showed that UTS increased consistently with an increase of nozzle temperature, and the maximum UTS was obtained at the infill angle of 45°. For UTS, the relative influence of processing parameters followed the order: nozzle temperature ≈ printing speed > raster angle > layer thickness.

Interestingly, both BT and SR increased significantly with increasing layer thickness.

Zhen et al. [37] applied different extrusion rates, raster angles, printing orientations and post-processing heat treatments to tune the crystallinity and strength of FFF-PEEK parts. After annealing at 300 °C for 2 hours, the resulting UTS reached approximately 80% of that of injection-molded PEEK parts. Notably, horizontal printing with ±10° raster angle or vertical printing with ±20° raster angle yielded the best mechanical performance among the results from all test conditions. Overall, horizontally printed coupons exhibited reduced warpage compared to vertically printed ones.

To summarize, in our compiled dataset, a wide range of FFF parameter combinations were investigated, and all studies reported UTS values, enabling direct process-property comparison across 12 different data sources. By analyzing this diverse dataset, we aim to identify the most influential processing parameters —and their interactions —that govern the UTS of the FFF-printed PEEK coupons.

3 METHODS AND RESULTS

The overall workflow of this literature-driven meta-analysis is shown in Figure 4.

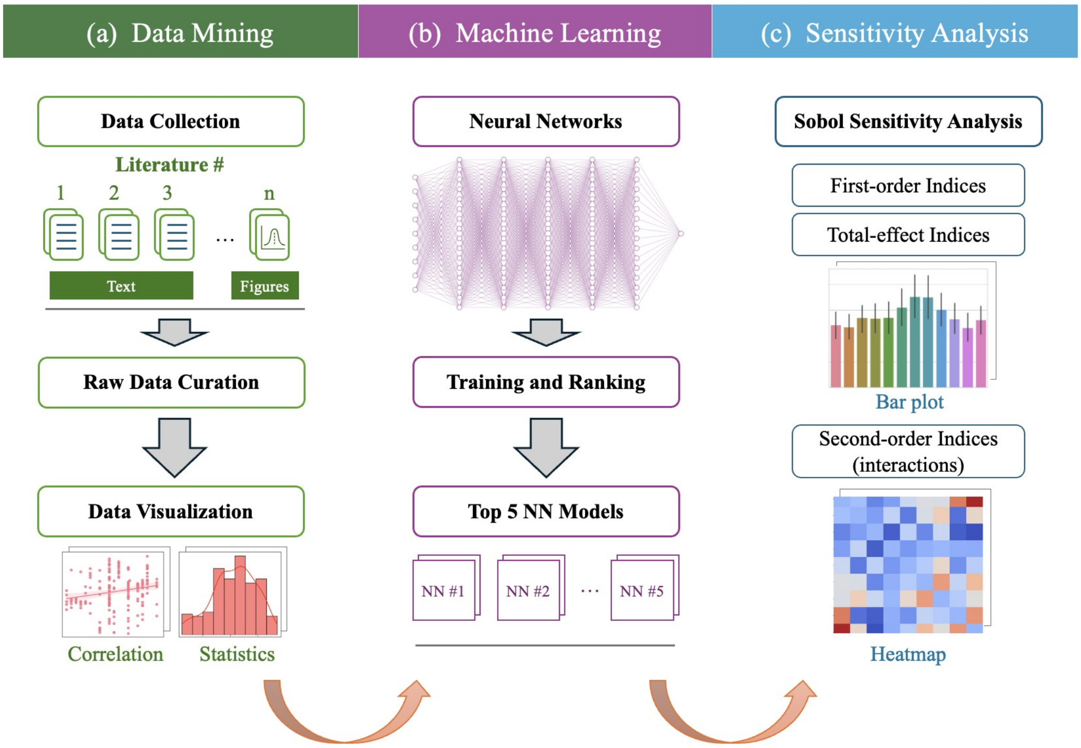

Figure 4 Workflow of this literature-driven meta-analysis on FFF with PEEK: (a) Data Mining, (b) Machine Learning, (c) Sensitivity Analysis using Sobol's method

The steps are summarized as follows:

a) Data Mining:

i. **Data Collection:** As previously introduced, we extract the data points from the twelve source studies that report the UTS of PEEK coupons fabricated by FFF.

ii. **Raw Data Curation:** Only horizontally printed samples, as shown in Figure 2(b), are selected from each study. Missing values for the FFF process parameters are estimated

 VOR: doi.org/10.1016/j.jmapro.2026.02.044

(imputed) using values from other literature sources, machine instructions, or material Technical Data Sheet (TDS), to the best of the authors' knowledge.

iii. **Data Visualization:** After preprocessing on the 3D-printing parameters, we visualize the relationships between individual 3D-printing parameters and the target response (UTS) as a parametric study. The statistical distribution of UTS from all data points is shown using box plots and histograms.

b) Machine Learning:

To further understand the relationship between the processing parameters and UTS, thousands of fully connected feedforward NNs are trained by varying hyperparameters and network architecture. Five top NN models are combined into an ensemble NN model for improved robustness in prediction tasks. The NNs are used not only for prediction but as surrogate models enabling explainable global sensitivity analysis.

c) Sensitivity Analysis:

To investigate how input uncertainty affects UTS variance, we apply explainable AI via Sobol global sensitivity analysis using the trained NN surrogates [38, 39].The top performing NN models are used collectively to conduct Sobol sensitivity analysis. Both the first-order and total-effect Sobol indices are calculated for all nine 3D-printing parameters. This approach reduces the biases from any single predictive NN model and provides a more comprehensive view of parameter importance. First-order and total-effect indices are used to study direct effects from coupled interactions.

3.1 Data Mining

3.1.1 Data Collection

The data points are collected from recently published literature [10, 11, 13-15, 29, 31-34, 36, 37] in the field of FFF/FDM using PEEK. The cut-off date for this data collection is the end of 2023, with the earliest data available starting from 2018. Although some data were available before 2018, we decided to focus on more recent experimental data that have better representation of the current state-of-the-art and material formulation. The selection includes a preference for 3D-printed tensile coupons with reported UTS. One of the coupon geometries using ASTM D638 Type I is shown in Figure 3.

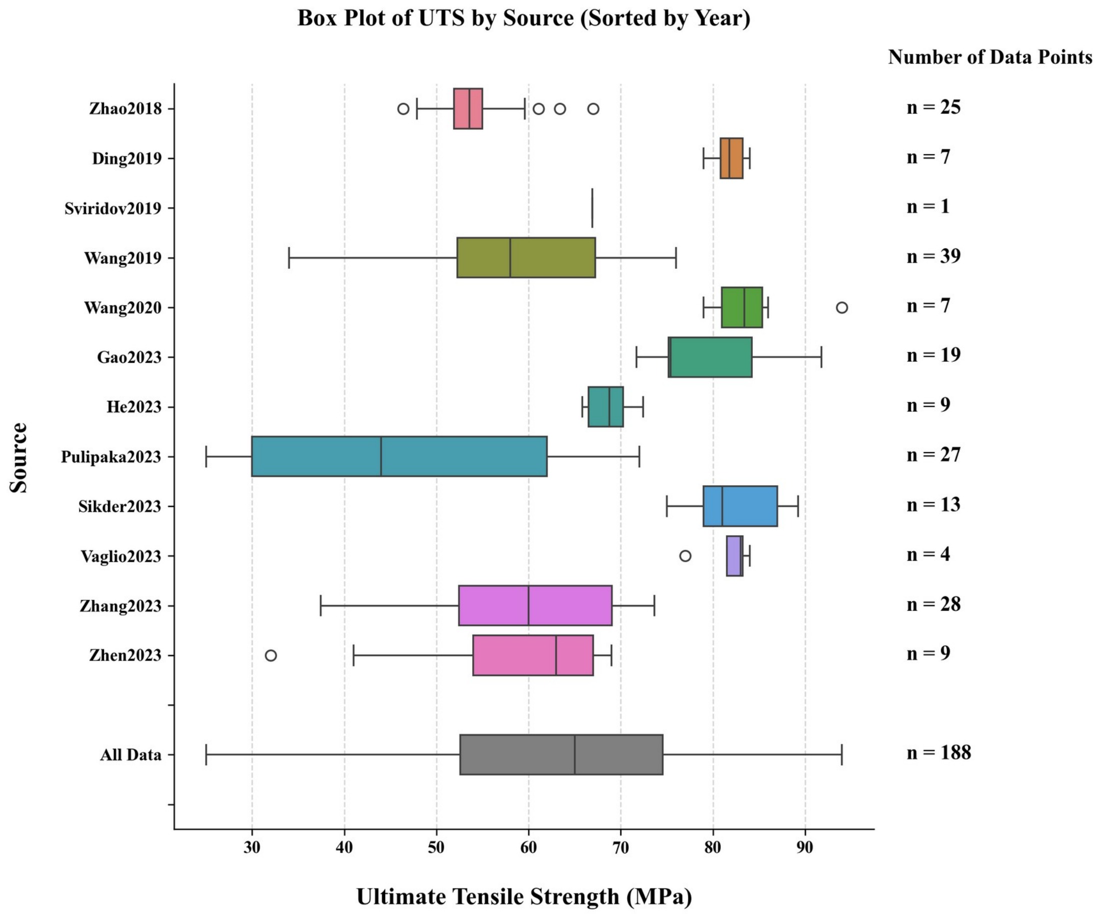

Figure 5 Box plot of UTS by source, sorted by year of publication

Figure 5 presents a summary plot of UTS values reported by 12 different studies, each employing various 3D printing process conditions. The plot highlights substantial variability in UTS values not only between studies but also within individual sources. These uncertainties could be attributed to different values, ranges and combinations of FFF process parameters. Some of these are illustrated in Figure 1, such as nozzle temperature, printing speed, layer thickness, and so on. It is worth noting that there are other uncertainty sources not specifically included in this literature survey, such as differences in material batches, 3D printers, post-annealing details and tensile testing protocols. Some studies (e.g., Pulipaka2023 [11]) reported a relatively wide range of UTS values, indicating either diverse processing conditions or an exploratory DOE. In contrast, Ding2019 [31] and Wang2020 [33] reported narrow UTS ranges, possibly reflecting controlled testing condition or small variations in the 3D-printing parameters. The "All Data" in Figure 5 gives a statistical distribution of all 188 data points in this dataset, underscoring the challenge of benchmarking mechanical properties of FFF-printed PEEK tensile coupons.

For the filament material, PEEK 450G, a grade of unfilled PEEK, is often cited or assumed in most studies. The properties of this specific PEEK material are summarized in Table 1, compiled from commercial PEEK technical data sheets [40, 41].

Table 1 Material Properties of PEEK 450G

Material Property	Notation	Nominal Value

Melting Point	T_m	343 ℃
Glass Transition Temperature	T_g	143-150 ℃
Density	ρ	1.30 g/cm^3
Ultimate Tensile Strength	UTS or σ_{uts}	98-100 MPa
Tensile Modulus	E	3.7-4 GPa

Generally, different studies have different preferences in the selection of printing parameters, thus posing a great challenge to curate the dataset for machine learning purposes. Nonetheless, from the available data in this collection, we hand-picked 9 printing parameters (e.g., nozzle temperature, layer thickness, printing speed, raster angle) as shown in Figure 1, and listed in Table 2. A summary of collected values and ranges of 3D-printing parameters is shown in Table 2. Overall, 188 data points are collected from 12 different sources, and some values of printing parameters have been imputed if not reported directly in the original experimental studies on FFF-PEEK.

Table 2 Summary of printing parameters from different data sources

No	Source	Year	Nozzle Temp (C)	Printing Speed (mm/sec)	Layer Thickness (mm)	Nozzle Diameter (mm)	Platform Temp (C)	Build Time* (min)	Specimen Thickness (mm)	Infill Percentage (%)	Raster Angle (deg)
1	Zhao [13]	2018	355 - 375	30	0.2	0.4	230 - 270	23	4	100	±45°
2	Ding [31]	2019	360 - 420	20	0.2	0.4	270	98.0	4	Not reported	±45°
3	Sviridov [32]	2019	450	40	0.25	0.7	290	33	4	100	±45°
4	Wang [29]	2019	380 - 440	17 - 26	0.1 - 0.5	0.4 - 0.8	280	37.7 - 196	4	Not reported	±45°
5	Wang [33]	2020	440	15	0.2	0.4	260	129	4	100	±45°
6	Sikder [34]	2023	380 - 410	30 - 50	0.1 - 0.3	Not reported	100 - 130	9.3 - 28	4	100	Not reported
7	Gao [10]	2023	390 - 420	20 - 50	0.1 - 0.25	0.4	125 - 140	12.4 - 77.5	4	100	Not reported
8	He [14]	2023	420 - 440	30 - 50	0.1 - 0.2	0.4	100 - 120	8.0 - 25.0	3	100	0°
9	Pulipaka [11]	2023	390 - 420	15 - 25	0.1 - 0.3	0.4	136 - 150	44 - 235	3.2	70 - 100	±45°
10	Vaglio [15]	2023	380 - 420	15- 65	0.1 - 0.2	0.4	145	4.27 - 37	2	100	±45°
11	Zhang [36]	2023	420 - 450	60 - 90	0.1 - 0.3	0.4	140	14.7 - 66	3	100	0°, 90°, ±45°
12	Zhen [37]	2023	430	40	0.2	0.4	Not reported	51	4	Not reported	±10°, ±20°, ±30°, ±45°

* Build time of each tensile coupon was re-calculated by creating the CAD models in Abaqus and then exporting to

 VOR: doi.org/10.1016/j.jmapro.2026.02.044

a slicing software Intamsuite V4.3 [28], assuming the use of a consistent 3D printer: Intamsys Funmat HT.

Other parameters like chamber temperature, addition of carbon fiber or glass fiber, post-annealing temperature, and hold time are ignored in this study due to insufficient data. More details of preprocessing are provided in **3.1.2.

3.1.2 Raw Data Curation

To support machine learning model training, the raw dataset was carefully preprocessed. Unreported data were imputed using engineering estimates based on the most frequently observed values in the literature, material TDS, or 3D printer instructions. Table 3 summarizes the imputed values assigned to each printing parameter.

Table 3 Preprocessing of 3D-printing parameters

3D-printing parameter	Assumed Value if Unreported
Nozzle temperature	All reported
Printing speed	All reported
Layer thickness	All reported
Build time*	Re-calculated using slicing software INTAMSUITE v4.3 [28]
Specimen thickness	All reported
Nozzle diameter	0.4 mm, assumed for Sikder [34]
Platform temperature	130 ℃, assumed for Zhen [37]
Infill percentage	100%, assumed for Ding [31], Wang [29] and Zhen [37]
Raster angle	±45°, assumed for Gao [10] and Sikder [34]
The following parameters were omitted in the analysis due to insufficient data in the compiled dataset.	
Chamber temperature	Reported in Zhao [13], Sikder [34], Gao [10], He [14], Pulipaka [11], Vaglio [15], Zhang [36]
Post-annealing temperature and hold time	Reported in Gao [10], Zhen [37], He [14], Sikder [34], Zhang [36]
Addition of carbon or glass fiber	Reported in Wang [33]
Extrusion rate	Reported in Zhen [37]

3.1.3 Data Visualization

As shown in Figure 6, a parametric study was conducted by plotting each printing parameter against the UTS. Some general trends are revealed in these subplots using linear regression lines.

FFF parameters such as nozzle temperature and infill percentage are positively correlated with UTS. As previously reported by Raj et al. [42], even small changes in the temperature of the material, could significantly affect the melt viscosity of PEEK. For example, the PEEK melt viscosity decreases from about 800 $Pa \cdot s$ to about 50 $Pa \cdot s$ as the temperature increases from 370 ℃ to 430 ℃. The high viscosity at 370 ℃, significantly limits the melt-flow capability of PEEK and may lead to insufficient fusion between adjacent layers. This results in more and larger voids, severely reducing the interlayer bonding strength and other mechanical properties. Further discussions on the effect of nozzle temperature on UTS can be found in [29, 31].

However, nozzle temperature is not the only factor that determines the behavior of the material once the PEEK extrudes from the nozzle tip. Other parameters such as platform (bed) temperature [30], chamber temperature [30], and fan speed [12] also contribute to the cooling rate, temperature history, crystallinity, and viscosity of the material at specific times and locations, thereby influencing the resulting bulk mechanical properties (e.g., UTS).

Infill percentage, although showing a general positive effect on UTS in Figure 6, exhibited different behavior in a specific study by Pulipaka et al. [11]. Counterintuitively, the maximum UTS was observed at an infill percentage of 85%, and the 75% infill produced a higher UTS than 100% infill. Nonetheless, infill percentage accounted for an 86.4% contribution to the UTS of FFF-printed PEEK, according to their ANOVA results.

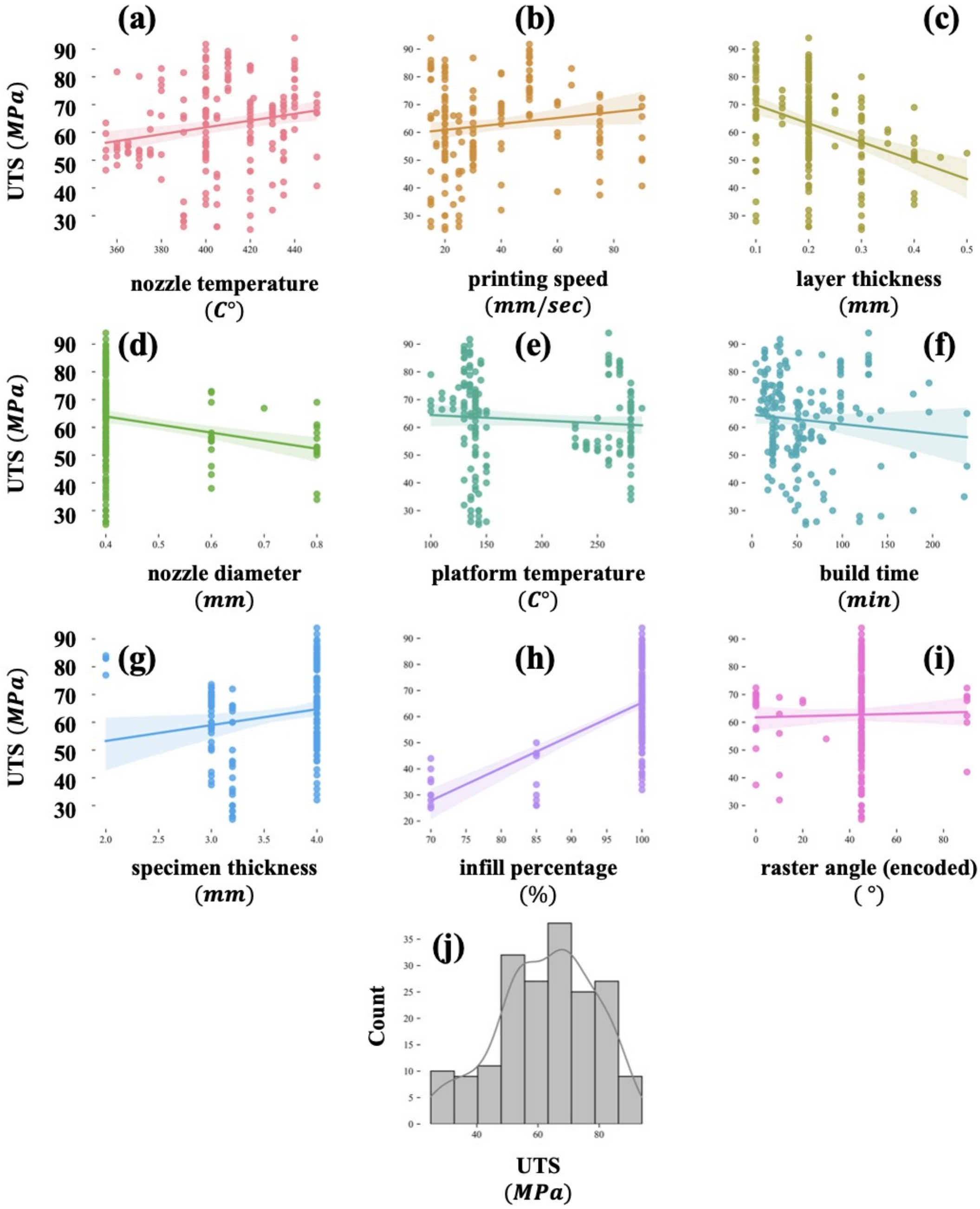

Figure 6 Visualization of a parametric study after preprocessing the 9 input parameters from the 3D-printing process. The first 9 subplots represent the individual relationships between the UTS and each 3D-printing parameter. The last subplot in the bottom row shows the histogram of the distribution of tensile strength values reported in this dataset, based on 188 data points.

In the meantime, layer thickness and nozzle diameter appear to be negatively impacting the UTS (Figure 6). Similar results are reported by Wang et al. [29], Gao et al. [10], and Pulipaka et al. [11]. It is believed that the thinner the layer thickness, the lower the chance of forming defects and air pores during the 3D-printing process, and the better the interlayer bonding strength.

Wang et al. [29] also reported that, when using a nozzle diameter of 0.6 mm or 0.8 mm, a layer thickness equal to or greater than 0.35 mm would interrupt the compaction and bonding strength of interlayers, leading to stratification and lower tensile strength of PEEK parts. However, the 0.4 mm nozzle produced little change in tensile strength when changing the layer thickness from 0.1 to 0.25 mm.

Some FFF printing parameters do not show a noticeable impact in these subplots, such as printing speed, platform temperature, build time, specimen thickness and raster angle. Specimen thickness, previously not investigated as frequently as nozzle temperature or printing speed, shows a slight positive effect on UTS in Figure 6.

These qualitative trends with limited interpretability are expected as we are superposing all the 3D-printing parameters and outcomes on these subplots. Therefore, more quantitative measures are required to better understand the individual impact of each FFF parameter on the UTS, and the correlations between these FFF parameters.

3.2 Machine Learning by Neural Networks

3.2.1 Neural Network Architecture and Training Protocol

To build a machine learning model for regression purposes and subsequent sensitivity analysis, we train feedforward fully connected NN models. Multiple combinations of hyperparameters—such as learning rate, number of hidden layers, nodes per layer, batch size, and activation function—were systematically varied as summarized in Table 4 to explore model performance and ensure robustness. A sample structure of an NN with 1 input layer, 5 hidden layers and 1 output layer is shown in Figure 7. Each NN takes nine FFF process parameters as inputs and predicts the UTS.

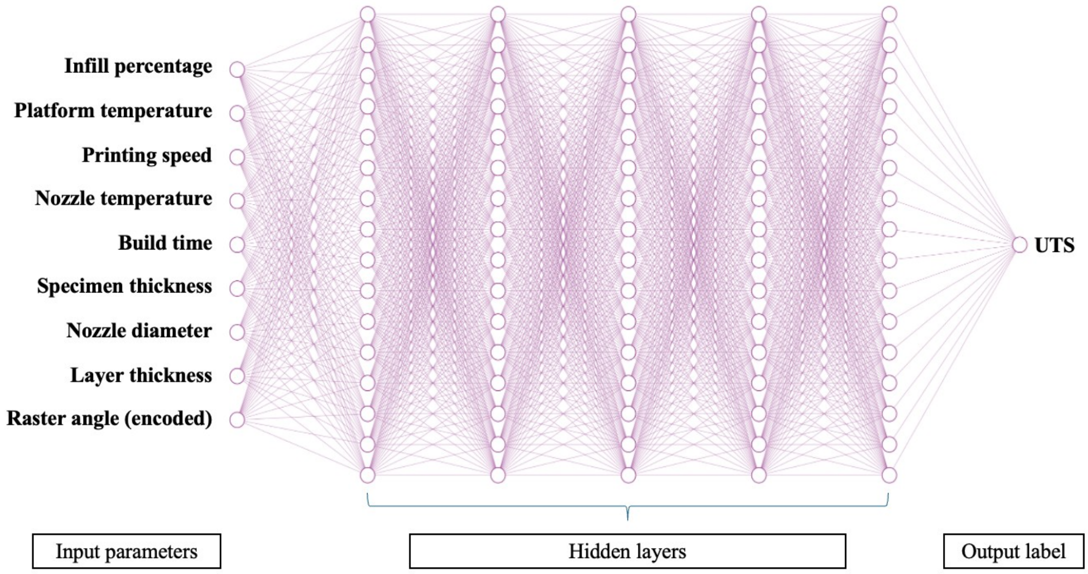

Figure 7 A sample structure of a neural network with 9 input parameters from the 3D-printing process (on the left-hand side), and UTS as the single output response (on the right-hand side). This architecture contains 1 input layer, 5 hidden layers and 1 output layer.

As shown in Table 4, all 188 data points are split into training, validation, and test datasets. The test size is 10% of the total data points and rounded up to 19 data points. The test data is kept outside of the NN training loop and is not used until all the training is done. This helps mitigate overfitting of the NN models. During the training, the initial training block is further divided into 90% training and 10% validation set, which are 81% and 9% of the total data points. Adam (Adaptive Moment Estimation) is chosen as the optimizer, which adapts the learning rate for each parameter by keeping track of both the average of recent gradients (momentum) and the average of recent squared gradients (RMS).

Table 4 Hyperparameters for Neural Networks

Hyperparameter	Value
Training size	0.9*0.9 = 81% (152 data points)
Validation size	0.9*0.1 = 9% (17 data points)
Test size	10% (19 data points)
Random state	42
Optimizer	Adam
Number of hidden layers	5, 7
Number of nodes in each hidden layer	16, 32, 64, 128, 256
Epoch	100, 200, 300, 600
Batch size	16, 32
Activation function	Tanh, Relu, Elu
Learning rate	0.01, 0.005, 0.001, 0.0005, 0.0001
Loss function	Mean squared error (MSE)
Metrics	Mean absolute error (MAE)

Grid-search is conducted throughout the NN training, and every model is saved after each training. Overall, 1,200 different NN models are trained and ranked by testing scores (R^2_{test}). RMSE and MAE are also recorded for each NN model training and testing. The mathematical formulations of these evaluation metrics are shown below:

$$R^2 = 1 - \frac{\sum_{i=1}^{n}(y_i - \hat{y}_i)^2}{\sum_{i=1}^{n}(y_i - \bar{y})^2} \quad (1)$$

$$RMSE = \sqrt{\frac{1}{n}\sum_{i=1}^{n}(y_i - \hat{y}_i)^2} \quad (2)$$

$$MAE = \frac{1}{n}\sum_{i=1}^{n}|y_i - \hat{y}_i| \quad (3)$$

Where:

- y_i: true value at position X_i
- $\hat{y}_i$: predicted value at X_i
- $\bar{y}$: mean of all the true values
- n: number of total data points

Interpretation:

- $R^2 = 1$: perfect prediction
- $R^2 = 0$: model predicts no better than the mean
- $R^2 < 0$: model is worse than just predicting the mean
- $RMSE \vee MAE = 0$: perfect prediction; Otherwise, less than perfect

 VOR: doi.org/10.1016/j.jmapro.2026.02.044

The models are implemented using scikit-learn [43] and TensorFlow [44] Python libraries. Common python libraries like NumPy, pandas, Matplotlib and seaborn are also used. Training time varies depending on the learning rate and number of epochs, typically ranging from 1 to 20 seconds on a desktop computer with an Intel Core i9-12900K CPU (16 cores), Nvidia RTX A2000 GPU (12 GB VRAM), and 96 GB of DDR5-4400 MHz memory. Within each training loop, training history and scores are saved in a separate subfolder, enabling post-processing once all training is completed.

3.2.2 Results from Neural Networks

After training 1,200 NNs using a grid-search with the hyperparameter dictionary detailed in Table 4, the models are ranked by R^2_{test} scores. A filtering criterion of $R^2_{train} > 0.90$ and $R^2_{test} > 0.85$ is applied to identify well-generalized models. The hyperparameters and performance metrics of the top 5 NN models are summarized in Table 5.

Table 5 Hyperparameters and Scores of the top NN models

Nodes	Hidden Layers	Learning Rate	Epochs	Batch Size	Activation Function	R^2_{train}	R^2_{test}	$RMSE_{tra}$ (MPa)	$RMSE_{tes}$ (MPa)
128	5	0.01	200	32	elu	0.922	0.894	5.85	4.67
128	7	0.005	200	16	elu	0.910	0.894	5.86	4.57
64	7	0.005	200	32	elu	0.911	0.890	5.97	4.34
64	5	0.01	200	32	elu	0.912	0.888	6.01	4.76
256	7	0.001	600	16	elu	0.915	0.887	6.05	4.78

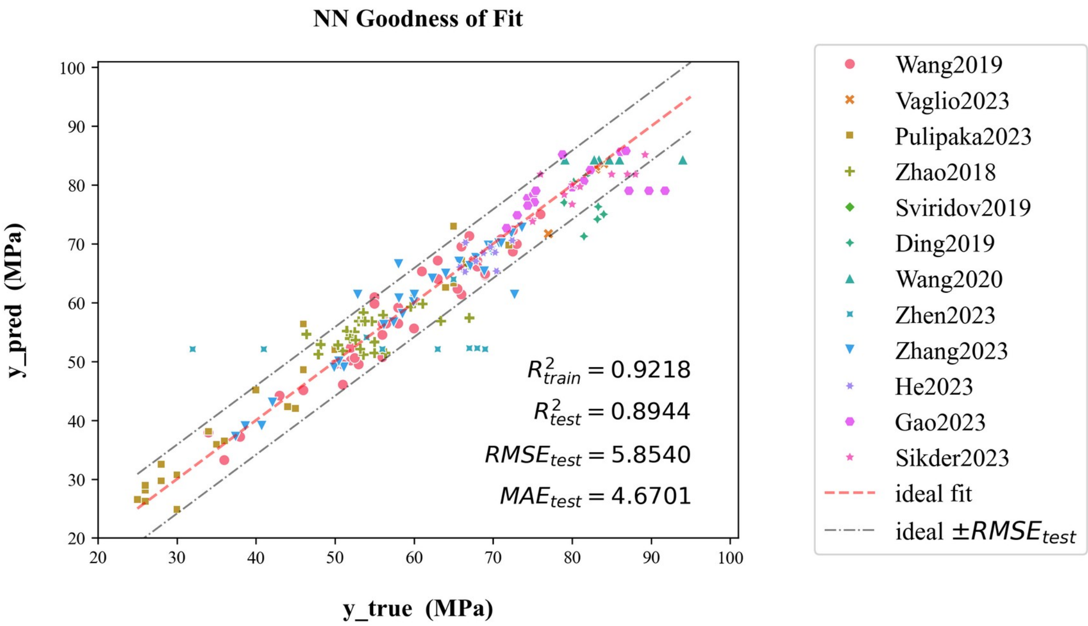

Figure 8 Goodness-of-fit for the top-performing neural network model based on test data evaluation.

To understand the goodness-of-fit of the NN models, we plot out the predicted vs true UTS values for all 188 data points using one of the top performing models, as shown in Figure 8. Most predictions are accurate and cluster closely around the red dashed line, representing the ideal fit. Two gray dot-dashed lines indicate the bounds defined by the $RMSE_{test}$ of the NN model. As observed, most prediction points in Figure 8 fall within these bounds. However, some points—particularly from the studies by Gao2023 [10], Wang2020 [33] and Zhen2023 [37] —exhibit horizontal scatter. This discrepancy can be attributed to the omitted process parameters in the NN training, such as post-annealing temperature and hold time (Gao2023 [10]), fiber reinforcement content (Wang2020 [33]), and extrusion rate (Zhen2023 [37]). Given the limited dataset size, it is impractical to include all possible process variables in the NN training to achieve high predictive performance.

3.3 Global Sensitivity Analysis by Sobol's Method

3.3.1 Sobol Sensitivity Analysis Methodology

To investigate how the uncertainty in the inputs affects the variance of the target response, sensitivity analysis using Sobol's method is applied. Neural networks are trained as surrogate models, enabling fast predictions for the thousands of evaluations required to compute Sobol indices. An introduction to Sobol sensitivity analysis can be found in the literature [38, 39], and an intuitive representation is available in [45]. A specific Python library, SALib [46], is used to compute the first-order, second-order and total-effect Sobol indices of all 9 printing parameters, using the trained NN models from Section **3.2**. A total of 4096 runs is set in SALib—four times the recommended 1024 runs—to ensure convergence and numerical stability. For Sobol indices, the first-order index of an input parameter quantifies the proportion of the output variance explained by that parameter alone. The total-effect index includes the first-order contribution plus all interaction effects involving that parameter.

Mathematically, using ANOVA-HDMR decomposition for $Y=f\left(x_1,x_2,\ldots,x_k\right)$:

$$V\left(Y\right)=\sum_i V_i+\sum_i\sum_{j>i}V_{ij}+\ldots+V_{12\ldots k} \quad (4)$$

where:

- $V\left(Y\right)$ is the total variance of output feature Y.
- V_i , the first-order term, represents the portion of the response (Y) to x_i when only varying x_i a Monte Carlo simulation.
- V_{ij} is the interaction term between x_i and x_j ($i\neq j$). It captures the part of the response of Y to x_i, x_j) that cannot be explained separately by x_i and x_j.
- $V_{12\ldots k}$ is the interaction term among all the input factors $\left(x_1,x_2,\ldots,x_k\right)$.

By dividing both sides of the variance decomposition equation by the total variance $V\left(Y\right)$, we obtain:

$$\sum_i S_i+\sum_i\sum_{j>i}S_{ij}+\sum_i\sum_{j>i}\sum_{k>j}S_{ijk}+\ldots+S_{12\ldots k}=1 \quad (5)$$

where (assuming k =3):

- First-order sensitivity index:

 VOR: doi.org/10.1016/j.jmapro.2026.02.044

$$S_1 = S_1 \quad (6)$$

- Second-order interactions:

$$\sum_{j>1} S_{1j} = S_{12} + S_{13} \quad (7)$$

- Third-order interactions:

$$\sum_{j>1} \sum_{k>j} S_{1jk} = S_{123} \quad (8)$$

- Total-effect index:

$$S_{1_{total}} = S_1 + S_{12} + S_{13} + S_{123} \quad (9)$$

when the total number of input variables $k = 3$.

3.3.2 *Results from Sobol Sensitivity Analysis*

Sobol sensitivity indices are computed and aggregated from the top 5 NN models simultaneously using an ensemble approach. As shown in Figure 9, the first-order and total-effect Sobol indices of 9 FFF printing parameters are plotted in a bar plot with error bars (± 1 standard deviation). Based on the first-order indices alone, the printing speed, infill percentage, build time and platform temperature are the most significant parameters affecting the variance in the tensile strength of 3D-printed PEEK coupons. However, the total-effect indices reveal that the remaining parameters also contribute significantly through interactions. The large gaps between first-order and total-effect values for many variables underscore strong interaction effects among parameters. This highlights the inherent complexity of optimizing multiple process parameters simultaneously.

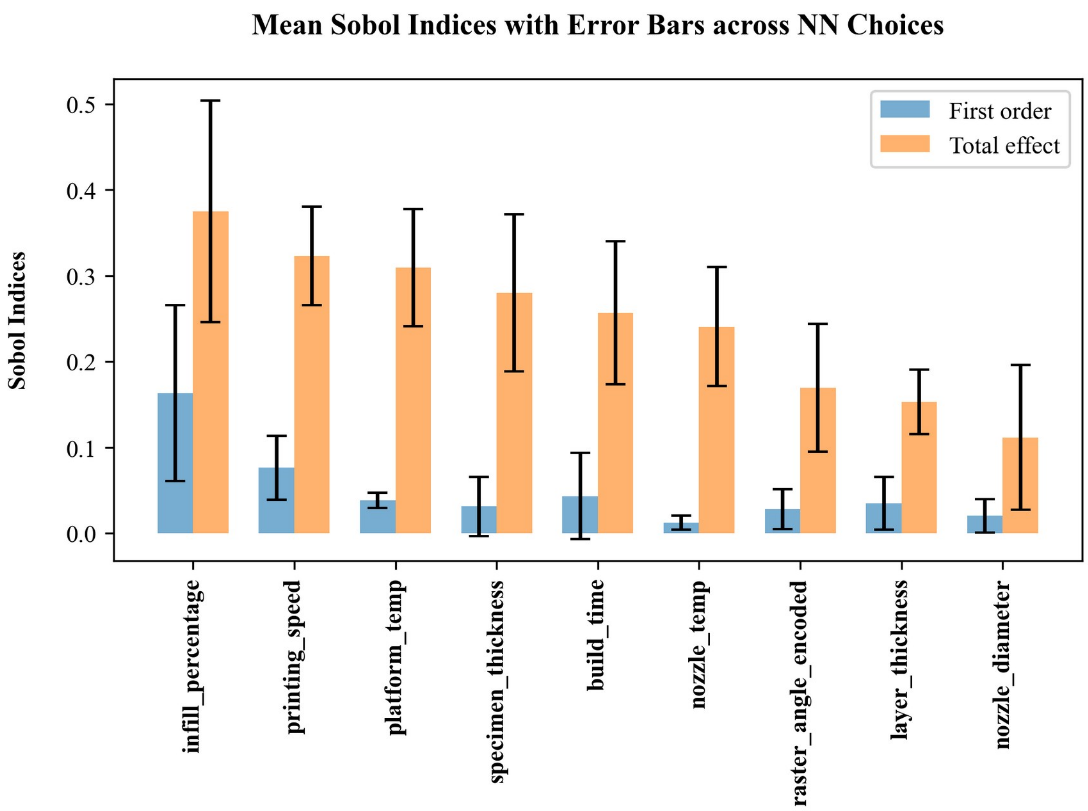

Figure 9 Sobol sensitivity analysis using the top five NN models. The blue and orange bars represent the mean first-order and total-effect Sobol indices, respectively. Error bars indicate ±1 standard deviation, calculated using

the SALib library [46].

These Sobol sensitivity analyses results indicate that, while certain FFF printing parameters such as infill percentage and printing speed exert dominant first-order effects, most of the input features demonstrate strong interactions, as evident from the large discrepancies between their total-effect and first-order indices. For example, nozzle temperature, which is traditionally considered critical in isolation, ranks only moderately based on its first-order index but exhibits a high total-effect index. This finding implies that nozzle temperature is influential primarily through its interactions with other parameters like layer thickness and platform temperature, rather than through its direct effect. Such coupling of parameter effects is indicative of the multi-physics complexity underlying the FFF process. Ultimately, the analysis confirms that optimizing individual parameters in isolation may be insufficient, and a multi-variable co-optimization strategy is necessary to improve print quality and mechanical performance.

Furthermore, we visualize the averaged second-order Sobol indices in a heatmap, as shown in Figure 10. As shown, most second-order indices are close to zero, indicating weak interaction between most pairs of FFF printing parameters. The largest averaged interaction effects are observed between build time and specimen thickness (0.023), build time and raster angle (0.018), printing speed and platform temperature (0.016), raster angle and specimen thickness (0.016), and platform temperature and specimen thickness (0.013), suggesting that simultaneous adjustment of these parameter pairs may be important for optimizing experimental outcomes.

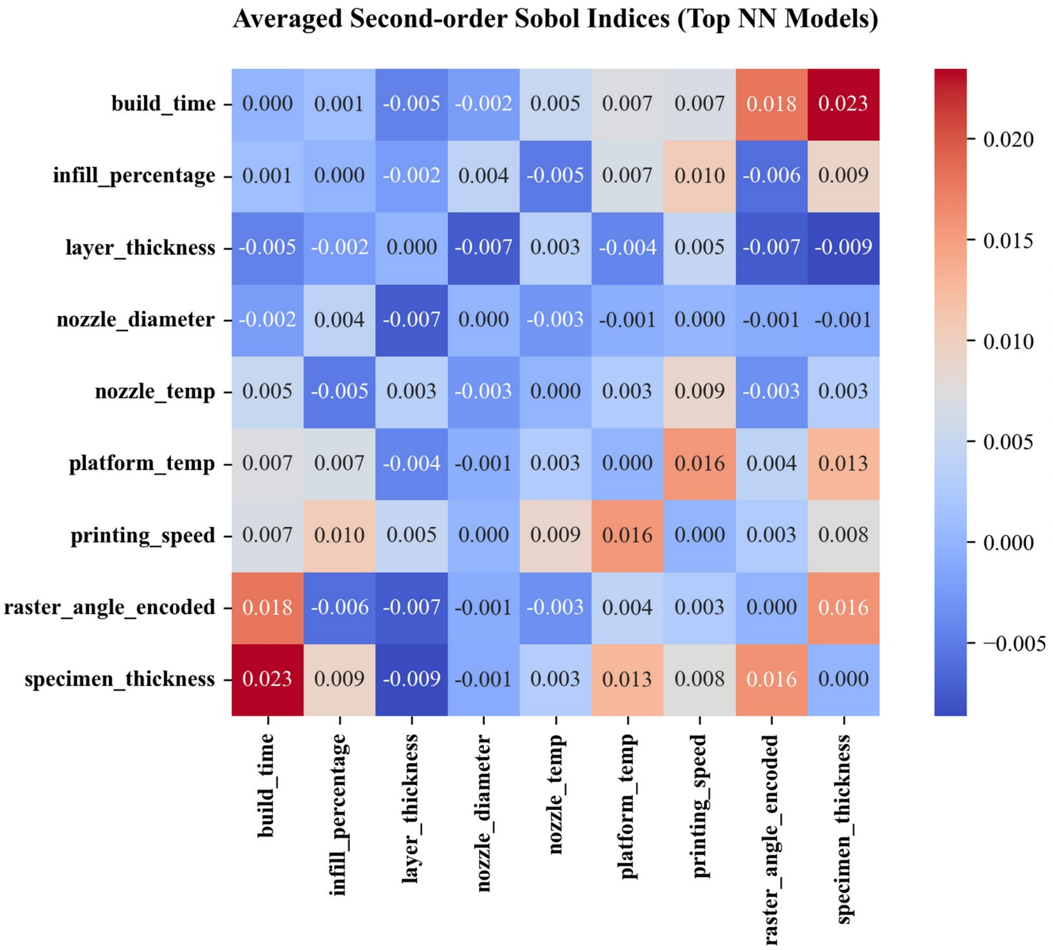

Figure 10 Averaged second-order Sobol Indices computed using the top five NN models

4 DISCUSSIONS

Figure 5 and Figure 6 summarize first-order trends and variability in UTS for FFF-printed PEEK across twelve studies. Figure 5 provides a box plot comparison of UTS values across these literature sources, sorted by year of publication. The data exhibit substantial variability both between and within studies, underscoring the sensitivity of UTS to process parameters. For example, Pulipaka2023 [11] exhibits wide interquartile ranges while Ding2019 [31], He2023 [14] and Wang2020 [33] show much narrower ranges. Zhao2018 [13] reports much lower UTS values than Ding2019 [31], likely reflecting differences in processing conditions. The overall range of UTS spans from ~30 MPa to over ~90 MPa, as seen in the "All Data" summary box, emphasizing the importance of a systematic approach for process optimization. In Figure 6, the influence of nine FFF printing parameters on UTS is illustrated through scatter plots with regression trends. Parameters such as layer thickness and nozzle diameter show clear downward trends, suggesting that thinner layers and smaller nozzles (0.4 mm) tend to promote higher mechanical properties. Conversely, a greater infill percentage and overall specimen thickness, increases UTS. Notably, nozzle temperature shows a slightly increasing trend, consistent with the literature. Pulipaka et al. [11] showed that nozzle temperature effects are coupled with other parameters, indicating an optimal window rather than a monotonic trend.

The neural network models trained on the literature-derived metadata achieved R^2_{train} and R^2_{test} scores about 90%, demonstrating that despite the noisy and heterogeneous nature of the data, machine learning frameworks can capture coupled and nonlinear process-property relationships. To reduce model bias, we adopted an ensemble machine learning framework that trained over 1000 candidate networks, ranked them by test score, and aggregated the top five for Sobol sensitivity analysis.

The significant differences between first-order and total-effect Sobol indices across most parameters reveal strong higher-order interactions. This aligns with the known challenges in FFF, where thermal gradients, cooling rates, and interlayer fusion are affected simultaneously by multiple process parameters. Nozzle temperature, for instance, acts synergistically with other parameters such as platform temperature and layer thickness, influencing crystallinity, porosity, and interlayer bonding.

Some limitations arise from sparse data and missing process parameters in the published literature. Parameters such as chamber temperature, post-annealing conditions, and material batch variation were excluded from the present analysis for that reason. Chamber temperature, for example, was not reported in many of the source studies. This omission may explain why some data points (e.g., from Gao2023 [10], Zhen2023 [37]) show larger prediction errors. Moreover, imputation of missing values introduces additional uncertainty.

Overall, the results demonstrate that data-driven optimization strategies can effectively guide process parameter tuning in multi-physics, strongly coupled processes such as FFF-PEEK. For instance, processing conditions that combine moderate nozzle temperatures, thinner layers, and higher infill percentages are predicted to enhance mechanical performance. This framework can potentially be adapted for other material systems and additive manufacturing methods.

5 CONCLUSION

This study introduces an effective data-driven framework to investigate the process-property relationship in 3D-printed polymers, using FFF of PEEK as a case study. A dataset of 188 UTS values from 12 independent studies was compiled, capturing the effects of nine commonly reported 3D-printing parameters, such as nozzle temperature, layer thickness, printing speed, and infill percentage.

To analyze this sparse and heterogeneous metadata, we implemented a robust machine learning pipeline involving the training of 1200 neural networks with varying hyperparameters and architecture.

The top-performing models achieves strong predictive performance (both R^2_{train} and $R^2_{test} \approx 90\,\%$), demonstrating that machine learning can effectively model coupled, nonlinear process–property relationships even with literature-derived data.

The top five NN models were used in an ensemble approach to conduct global sensitivity analysis via the Sobol method. The results reveal that parameters such as printing speed and infill percentage contribute dominant first-order effects, while others such as nozzle temperature primarily influence UTS through higher-order interactions. These insights underscore the importance of multivariate parameter tuning for process optimization rather than isolated adjustments.

Overall, this work offers a scalable and transferable methodology for extracting insight from scattered experimental metadata in additive manufacturing. Additionally, it supports informed process optimization, uncertainty quantification and material qualification. Ultimately, it can be extended to other materials, properties, and printing techniques to reduce reliance on trial-and-error for additive manufacturing workflows. Coupling NN surrogates with Sobol XAI shifts this work from black-box prediction to interpretable, transferable process insight, supporting multivariate co-optimization rather than single-parameter tuning.

ACKNOWLEDGEMENTS

The authors thank the University of Washington in Seattle for providing facilities and resources.

Data availability statement

Source data are extracted from published studies cited in the References. The curated dataset (188 data points) is available under a CC BY or CC0 license: https://doi.org/10.5281/zenodo.16815549

Author Contributions

Huilong Fu: Conceptualization, Data curation, Formal analysis, Investigation, Methodology, Software, Validation, Visualization, Writing – original draft, Writing – review & editing.

Navid Zobeiry: Conceptualization, Funding acquisition, Project administration, Supervision, Writing – review & editing.

All authors have read and approved the final manuscript and agree to be accountable for all aspects of the work.

Competing Interests

The authors declare no competing interests.

Funding

No funding was received for this work.

REFERENCES

1. Ngo, T.D., et al., *Additive manufacturing (3D printing): A review of materials, methods, applications and challenges.* Composites Part B: Engineering, 2018. **143**: p. 172–196.
2. Gao, W., et al., *The status, challenges, and future of additive manufacturing in engineering.* Computer-Aided Design, 2015. **69**: p. 65–89.
3. Hull, C., *Apparatus for production of three-dimensional objects by stereolithography*, in *U.S.*

Patent and Trademark Office. 1986: United State.
4. Kruth, J.P., et al., *Binding mechanisms in selective laser sintering and selective laser melting.* Rapid prototyping journal, 2005. **11**(1): p. 26–36.
5. Gokuldoss, P.K., S. Kolla, and J. Eckert, *Additive Manufacturing Processes: Selective Laser Melting, Electron Beam Melting and Binder Jetting—Selection Guidelines.* Materials, 2017. **10**(6): p. 672.
6. Gong, H., et al., *Analysis of defect generation in Ti–6Al–4V parts made using powder bed fusion additive manufacturing processes.* Additive Manufacturing, 2014. **1-4**: p. 87–98.
7. Doyle, M., et al., *Effect of Layer Thickness and Orientation on Mechanical Behavior of Binder Jet Stainless Steel 420 + Bronze Parts.* Procedia Manufacturing, 2015. **1**: p. 251–262.
8. Liu, Z., et al., *A critical review of fused deposition modeling 3D printing technology in manufacturing polylactic acid parts.* The International Journal of Advanced Manufacturing Technology, 2019. **102**(9): p. 2877–2889.
9. N. Turner, B., R. Strong, and S. A. Gold, *A review of melt extrusion additive manufacturing processes: I. Process design and modeling.* Rapid Prototyping Journal, 2014. **20**(3): p. 192–204.
10. Gao, J., et al., *Comprehensive Analysis of Fused Deposition Modeling Process Conditions for Enhancing Mechanical Properties and Surface Quality of 3d-Printed Poly-Ether-Ether-Ketone.* Available at SSRN 4612027, 2023.
11. Pulipaka, A., et al., *Effect of 3D printing process parameters on surface and mechanical properties of FFF-printed PEEK.* Journal of Manufacturing Processes, 2023. **85**: p. 368–386.
12. Lee, A., et al., *Effect of temperature history during additive manufacturing on crystalline morphology of PEEK.* Advances in Industrial and Manufacturing Engineering, 2022. **4**: p. 100085.
13. Zhao, F., D. Li, and Z. Jin, *Preliminary investigation of poly-ether-ether-ketone based on fused deposition modeling for medical applications.* Materials, 2018. **11**(2): p. 288.
14. He, Y., et al., *Effects of FDM parameters and annealing on the mechanical and tribological properties of PEEK.* Composite Structures, 2023. **313**: p. 116901.
15. Vaglio, E., et al., *Process parameters optimization in fused deposition modeling of polyether ether ketone.* Materials Research Proceedings, 2023. **35**: p. 182–190.
16. Borah, J. and M. Chandrasekaran, *Experimental investigation and development of Artificial neural network modeling of 3D printed PEEK bio implants and its optimization.* 2023.
17. Li, J., et al., *Multi-objective process parameters optimization of SLM using the ensemble of metamodels.* Journal of Manufacturing Processes, 2021. **68**: p. 198–209.
18. Garg, A., K. Tai, and M. Savalani, *State-of-the-art in empirical modelling of rapid prototyping processes.* Rapid Prototyping Journal, 2014. **20**(2): p. 164–178.
19. Poli, R., W. Langdon, and N. McPhee, *A Field Guide to Genetic Programming*. 2008, London: Lulu Enterprises UK Ltd.
20. Judd, C.M., G.H. McClelland, and C.S. Ryan, *Data analysis: A model comparison approach to regression, ANOVA, and beyond*. 2017: Routledge.
21. Bayraktar, Ö., et al., *Experimental study on the 3D‐printed plastic parts and predicting the mechanical properties using artificial neural networks.* Polymers for Advanced Technologies, 2017. **28**(8): p. 1044–1051.
22. Zhang, J., P. Wang, and R.X. Gao, *Deep learning-based tensile strength prediction in fused deposition modeling.* Computers in Industry, 2019. **107**: p. 11–21.
23. Cunningham, C.R., et al., *Invited review article: Strategies and processes for high quality wire arc additive manufacturing.* Additive Manufacturing, 2018. **22**: p. 672–686.
24. Doyle, L., et al., *Unraveling the Print–Structure–Property Relationships in the FFF of PEEK: A Critical Assessment of Print Parameters.* Polymers, 2025. **17**(11): p. 1444.
25. Wang, Y., et al., *Mechanical properties of fused filament fabricated PEEK for biomedical applications depending on additive manufacturing parameters.* Journal of the mechanical behavior of biomedical materials, 2021. **115**: p. 104250.
26. Liu, H., et al., *Experimental study on parameters of 3D printing process for PEEK materials.* IOP Conference Series: Materials Science and Engineering, 2019. **504**(1): p. 012001.
27. Gao, G., F. Xu, and J. Xu, *Parametric Optimization of FDM Process for Improving Mechanical Strengths Using Taguchi Method and Response Surface Method: A Comparative Investigation.* Machines, 2022. **10**(9): p. 750.
28. INTAMSYS, *INTAMSUITE v4.3*. 2024: https://www.intamsys.com/support-download-software?list=20.
29. Wang, P., et al., *Effects of printing parameters of fused deposition modeling on mechanical*

properties, surface quality, and microstructure of PEEK. Journal of Materials Processing Technology, 2019. **271**: p. 62–74.
30. Qu, H., et al., *Influence of Thermal Processing Conditions on Mechanical and Material Properties of 3D Printed Thin-Structures Using PEEK Material.* International Journal of Precision Engineering and Manufacturing, 2022. **23**(6): p. 689–699.
31. Ding, S., et al., *Effects of nozzle temperature and building orientation on mechanical properties and microstructure of PEEK and PEI printed by 3D-FDM.* Polymer Testing, 2019. **78**: p. 105948.
32. Sviridov, A., I. Lopatina, and I. Kurganova. *3D-printed polyether ether ketone samples mechanical properties estimation*. in *IOP Conference Series: Materials Science and Engineering*. 2019. IOP Publishing.
33. Wang, P., et al., *Preparation of short CF/GF reinforced PEEK composite filaments and their comprehensive properties evaluation for FDM-3D printing.* Composites Part B: Engineering, 2020. **198**: p. 108175.
34. Sikder, P., B.T. Challa, and S.K. Gummadi, *A comprehensive analysis on the processing-structure-property relationships of FDM-based 3-D printed polyetheretherketone (PEEK) structures.* Materialia, 2022. **22**: p. 101427.
35. El Magri, A., et al., *Optimization of printing parameters for improvement of mechanical and thermal performances of 3D printed poly(ether ether ketone) parts.* Journal of Applied Polymer Science, 2020. **137**(37): p. 49087.
36. Zhang, H., et al., *A novel method to combine fused deposition modelling and inkjet printing in manufacturing multifunctional parts for aerospace application.* Journal of Materials Research and Technology, 2023. **24**: p. 4405–4426.
37. Zhen, H., et al., *Effect of 3D Printing Process Parameters and Heat Treatment Conditions on the Mechanical Properties and Microstructure of PEEK Parts.* Polymers, 2023. **15**(9): p. 2209.
38. Sobol′, I.M., *Global sensitivity indices for nonlinear mathematical models and their Monte Carlo estimates.* Mathematics and Computers in Simulation, 2001. **55**(1): p. 271–280.
39. Saltelli, A., et al., *Global Sensitivity Analysis. The Primer.* 2008: John Wiley & Sons Ltd.
40. 3DXTECH, *Technical Data Sheet: ThermaX™ PEEK 3D Printing Filament (Rev. 3.0)*.
41. Limited, V.M., *VICTREX™ PEEK Polymer 450G™ Technical Data Sheet*. 2024.
42. Raj, R., et al., *Process dependent interface strengthening, de-icing and EMI shielding performance in PEEK/CF laminates.* Materials Advances, 2023. **4**(18): p. 4180–4189.
43. Pedregosa, F., et al., *Scikit-learn: Machine Learning in Python.* Journal of Machine Learning Research, 2011. **12**: p. 2825–2830.
44. Abadi, M.ı., et al., *TensorFlow: Large-Scale Machine Learning on Heterogeneous Distributed Systems*. 2015, Google Research.
45. Rabitz, H., et al., *Efficient input—output model representations.* Computer Physics Communications, 1999. **117**(1): p. 11–20.
46. Herman, J. and W. Usher, *SALib: An open-source Python library for sensitivity analysis.* Journal of Open Source Software, 2017. **2**(9): p. 97.

VOR: doi.org/10.1016/j.jmapro.2026.02.044

Appendix: Data Summary Extended from Table 2.

No.	Source	Number of data points	Printer	Material	Nozzle Temp (°C)	Printing Speed (mm/s)	Layer Thickness (mm)	Nozzle Diameter (mm)	Platform Temp (°C)	Build Time (min)	Specimen thickness (mm)	Infill percentage (%)	Raster angle (degree)
1	Zhao2018	25	home-made	Victrex 450G granules	355 - 375	30	0.2	0.4	230 - 270	23	4	100	+-45
2	Ding2019	7	home-made	Junhua 450G	360 - 420	20	0.2	0.4	270	98.0	4	Not reported	+-45
3	Sviridov2019	1	TotalZAny Form950 Pro Hot+	Victrex 381G granules	450	40	0.25	0.7	290	33	4	100	+-45
4	Wang2019	39	home-made	Junhua 450G	380 - 440	17 - 26	0.1 - 0.5	0.4 - 0.8	280	37.7 - 196	4	Not reported	+-45
5	Wang2020	7	home-made	Jinlin Zhongyan 450G	440	15	0.2	0.4	260	129	4	100	+-45
6	Sikder2023	13	Funmat HT Enhanced by Intamsys	3DXTech Thermax PEEK Natural	380 - 410	30 - 50	0.1 - 0.3	Not reported	100 - 130	9.3 - 28	4	100	Not reported
7	Gao2023	19	Funmat HT by Intamsys	K10 by Kexcelled	390 - 420	20 - 50	0.1 - 0.25	0.4	125 - 140	12.4 - 77.5	4	100	Not reported
8	He2023	9	Magic-HT-L	Jilin Joinature	420 - 440	30 - 50	0.1 - 0.2	0.4	100 - 120	8.0 - 25.0	3	100	0
9	Pulipaka2023	27	CreatBot F160	3DXTech	390 - 420	15 - 25	0.1 - 0.3	0.4	136 - 150	44 - 235	3.2	70 - 100	+-45
10	Vaglio2023	4	Funmat HT by Intamsys	Unspecified	380 - 420	15- 65	0.1 - 0.2	0.4	145	4.27 - 37	2	100	+-45
11	Zhang2023	28	Funmat Pro 410 by Intamsys	Intamsys	420 - 450	60 - 90	0.1 - 0.3	0.4	140	14.7 - 66	3	100	0, 90, +-45
12	Zhen2023	9	Dadun BMF-450	Unspecified	430	40	0.2	0.4	Not reported	51	4	Not reported	+-10, +-20, +-30, +-45